Journal of Superconductivity and Novel Magnetism (2022) 35:2881–2888
https://doi.org/10.1007/s10948-022-06320-7

ORIGINAL PAPER

The Anisotropic Magnetocaloric Effect and Size-Dependent Magnetic Properties of Iron Particles

Ahmed N. Halool[1] · Samy H. Aly[1] · Sherif Yehia[2] · Fatema Z. Mohammad[1]

Received: 27 April 2022 / Accepted: 11 June 2022 / Published online: 6 July 2022

Abstract
We present a theoretical study on the anisotropic magnetocaloric effect and the size-dependent magnetic properties of Fe particles of radii in the range 25–150 Å. An observable increase has been found in the magnetization, of the low radii (25–75 Å) particles, by reducing the temperature to 4 K. The anisotropic isothermal change in entropy ΔS_m has been calculated by taking the difference between maximum ΔS_m along the easy [100] and hard [111] directions. The maximum anisotropic ΔS_m is 0.015 J/kg K for a field change of 500 Oe along the [100] direction. The ΔS_m temperature dependence exhibits a table-like plateau for small radii (25–75 Å) and in low fields below 300Oe. This enhances the relative cooling power (RCP) of the Fe element to be 8.11 J/kg for particles of 25 Å radius. Also, the calculation of anisotropic ΔT_{ad} was performed along the easy axis and showed an increase in the maximum value around 37% relative to the experimental conventional value.

Keywords Ordinary magnetocaloric effect · Anisotropic magnetocaloric effect · Superparamagnetism · Size-dependent magnetization · Relative cooling power (RCP)

1 Introduction

Magnetocaloric effect (MCE) has attracted much research, both from the physics and application viewpoints, since its discovery in 1881 [1–8]. The discovery of the MCE in iron [9] has opened the door to extensive research on a variety of compounds, including the transition metal rare earth compounds, in an attempt to find the best MCE materials that operate near room temperature [1–15].

The fast development of nanometer-scale electronics demands the development of future cooling systems that can operate in complex geometries in the nanoscale range. An increase in the saturation magnetization in transition elements has been reported, when particle size is reduced to the nano-scale, at very low temperatures [15–17].

Research efforts, both experimental and theoretical, have been reported on the conventional MCE in the 3d transition elements at low and high fields, e.g., [14, 16, 18]. On the other hand, the anisotropic MCE (AMCE) is of interest because an increase in the entropy change could be achieved by rotating the crystal, along a specific crystalline direction, without changing the magnetic field intensity. This property was studied first by Kuzmin and Tishin in $DyAlO_3$ [17].

The application of magnetocaloric materials, either ordinary or anisotropic, in magnetic refrigeration has been the subject of many papers [14, 18–23]; in particular, search for materials with magneto-volume coupling and first-order phase transition is currently an active research area. Other applications of MCE materials are in the domain of medicine, e.g., in treating hyperthermia and in drug delivery [15, 24–28], where nanoparticles could be used.

In the present work, we report on the anisotropic size-dependent magnetic properties and the anisotropic magnetocaloric effect of crystalline cubic Fe, for spherical particles of radii in the 25–150-Å range, and at temperatures up to T_c. A statistical mechanics-based model is used, in the current work, for calculating the size-dependent magnetic and magnetocaloric properties of Fe. This model has been successfully used in studying a host of magnetic properties of magnetic systems of different crystalline symmetries. Examples of those systems are hexagonal, tetragonal, and

✉ Ahmed N. Halool
Eldocahmed4@gmail.com; ahmednagy@du.edu.eg

[1] Department of Physics, Faculty of Science, Damietta University, New Damietta, Egypt

[2] Department of Physics, Faculty of Science, Helwan University, Cairo, Egypt

mixed-anisotropy systems [29–33]. The aforementioned magnetic properties of those systems include magnetization curves, magnetic susceptibility, energy, torque, and probability landscapes.

2 Model and Analysis

The interplay between different magnetic energies dictates the magnetic properties of a given magnetic system and the total energy is subsequently used in evaluating magneto-thermal and magnetocaloric properties using the well-known relations of statistical mechanics.

Many publications provide experimental values of the temperature dependence of the anisotropy constants: K_1, K_2, and K_3 of *Fe* [34–40]. There is almost an agreement between these references on the sign and order of magnitude of K_1; however, this trend is not found regarding the value and the sign of K_2 and K_3. Therefore, we preferred to use the Callen and Callen power law [41, 42] to calculate the temperature-dependent anisotropy constants. The Callen and Callen law has been checked and verified for elements, e.g., Fe and Co [41–44]. The values of K_1 and K_2, at very low temperatures, used in our model were obtained from the reference by Getzlaff [40]. Those values proved to simulate magnetization curves which are in fair agreement with the experimental magnetization curves along the [100], [110], and [111] directions.

The energy density E_T is given by Eq. (1), where E_a and E_z are the anisotropy and Zeeman energy densities respectively:

$$E_T = E_a + E_z \tag{1}$$

where, for cubic systems, E_a can be expressed as [45]:

$$E_a = K_0 + K_1 f + K_2 s + K_3 w \tag{2}$$

where:

$$\begin{aligned} f &= a_x^2 a_y^2 + a_y^2 a_z^2 + a_x^2 a_z^2, \\ s &= a_x^2 a_y^2 a_z^2, \\ w &= a_x^4 a_y^4 + a_y^4 a_z^4 + a_x^4 a_z^4 \end{aligned} \tag{3}$$

and $E_z = -H \cdot M_s$

We assume that the saturation magnetization vector is oriented at an angle θ with the z–axis and its projection on the x–y plane makes an angle φ with the x-axis which is chosen to be along the [100] direction of the cubic crystal. Hence, the M_s direction cosines are:

$\alpha_x = \sin\theta \cos\varphi$, $\alpha_y = \sin\theta \sin\varphi$, and $\alpha_z = \cos\theta$.

Using the dimensionless quantities:

$\varepsilon_T = V\beta E_T$, $\alpha = V\beta K_1$, $\gamma = V\beta K_2$, $\xi = V\beta K_3$, and $\varepsilon_z = V\beta H M_S$, we rewrite Eq. (1) as:

$$\varepsilon_T = af + ys + \xi w - \varepsilon_z \cos\psi \tag{4}$$

where V, β, and ψ are the volume, $1/k_B T$, and the angle between $\boldsymbol{H}$ and $\boldsymbol{M_s}$ respectively. The quantity ε_z is the ratio between the Zeeman and the thermal energies. As a result, the value of ε_z represents the relative strength of these two quantities [45]. Iron particles are assumed to be spherical in shape with radius r. The classical partition function is given by:

$$Z = \int_0^{\pi} \sin(\theta) d\theta \int_0^{2\pi} \exp\left(-\varepsilon_T\right) d\varphi \tag{5}$$

and is subsequently used to evaluate magneto-thermal and magnetocaloric quantities.

The isothermal change in the magnetic entropy is given by:

$$\left|\Delta S_m\right| = \sum_i \frac{\left(M_{i+1}(H_{i+1}, T_{i+1}) - M_i(H_i, T_i\right)}{T_{i+1} - T_i} \Delta H_i \tag{6}$$

where $M(H,T)$ is the isothermal magnetization along a specific crystalline direction.

Equation (6) could be casted to take the following form [8, 44–49]:

$$\Delta S_m(Tav) = \frac{\delta H}{2\delta T}(\delta M_1 + 2\sum_{k=2}^{n-1} \delta M_k + \delta M_n) \tag{7}$$

In the reference by Pecharsky et al. [49], the authors discuss the limitations that should be imposed on δT and δH in order for Eq. (7) to be valid. The same reference also discusses and comments on the analysis given in another reference [50] on the same subject.

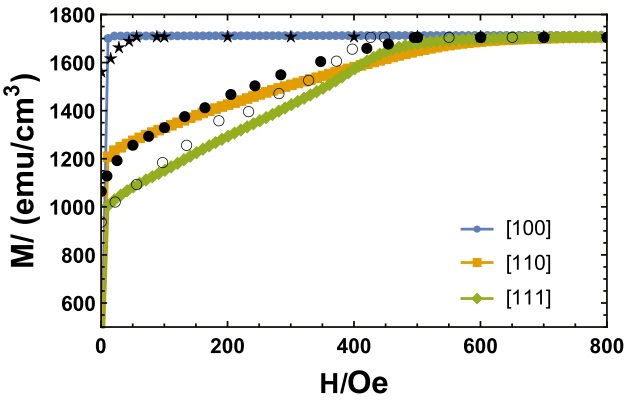

Fig. 1 The isothermal magnetization vs. magnetic field for Fe particles ($r = 150$ Å) at $H = 800$ Oe at room temperature. Our model (solid curves) experimental data (★ easy, · mid-hard, ○ hard directions)

The adiabatic change in temperature for a specific change in the external magnetic field is given by many references, e.g., [4, 7, 8, 12]:

$$\Delta T_{ad}(T,\Delta H) = -\int_{H_1}^{H_2} \frac{T}{C(T,H_F)}\left(\frac{\partial M(T,H)}{\partial T}\right)_H dH \tag{8}$$

However, one may write Eq. (8) in the following approximate form if the heat capacity is weakly field-dependent [8, 12]

$$\Delta T_{ad}(T,\Delta H) \approx \frac{-T}{C(T,H)}\Delta S_m(T,\Delta H) \tag{9}$$

A figure-of-merit called the relative cooling power (RCP) has been introduced to assess the performance of magnetocaloric materials. The RCP is determined by multiplying the magnitude of the maximum ΔS_m, at a definite field, times the difference in temperature, at full width at half maximum, of the ΔS_m vs. temperature curve as shown in the following equation [8] :

$$RCP = \Delta S_m^{\max} \times \delta T_{FWHM} \tag{10}$$

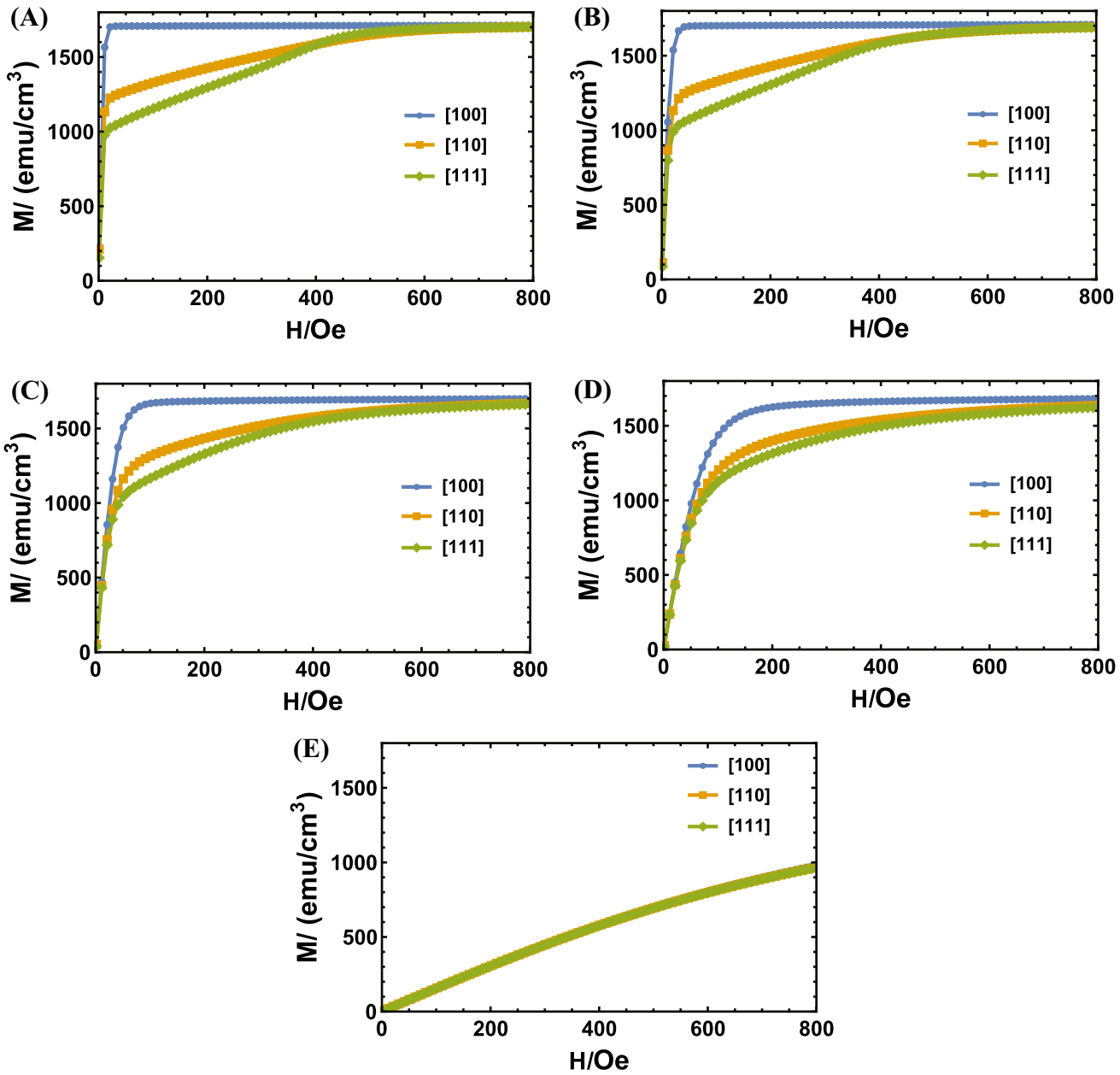

Fig. 2 The isothermal magnetization curves at 300 K for Fe particle of different sizes at **A** 125 Å, **B** 100 Å, **C** 75 Å, **D** 50 Å, and **E** 25 Å

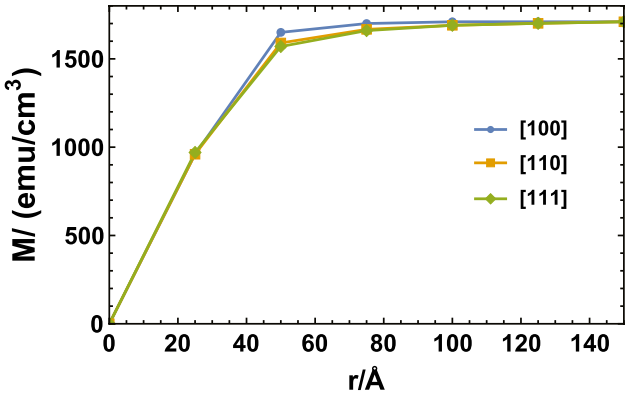

Fig. 3 Magnetization vs. particle size at 300 K and $H = 800$ Oe for particles of sizes in the 25–150-Å range

3 Results and Discussion

3.1 Size-Dependent Magnetization

Figure 1 shows the room temperature magnetization curves along the [100], [110], and [111] directions for a particle of radius $r = 150$ Å using our classical model. The saturation magnetization Ms is about 1713 emu/cm^3 (220.17 emu/g), i.e., very close to the experimental value of 217.2 emu/g as reported by Coey [52] and Kittel [53].

The sequence of the easy [100], mid-hard [110], and hard [111] directions is in agreement with the well-known data on cubic Fe crystals, e.g., [53, 54]. We have studied the effect of particle size on the magnetization curves for particles in the size range of 25–150 Å at room temperature. Figure 2A–E show the dependence of the magnetization curves on particle size in the range 25–125 Å. We noticed a relative decrease in the anisotropy between the [100] and [111] directions as the particle size is reduced (e.g., Fig. 2C). For a particle size of 25 Å, as shown in Fig. 2E, the magnetization curves along the three directions become identical and saturation (~ 1700 emu/cm^3) is far from being achieved in a field up to 800 Oe. Figure 3 displays the dependence of magnetization on particle size ($r = 25$–150 Å), at 300 K and in 800 Oe field. The magnetization drops considerably as the particle size is reduced below about 50 Å. This behavior is consistent with the experimental results on Fe [55–57] and other particles like Gd [29]. Figure 4A–D shows the isothermal magnetization curves parallel to the easy [100] axis for particles with radii in the 25- to 150-Å range and at temperatures 600, 400, 150, and 4 K, respectively. The field required to achieve

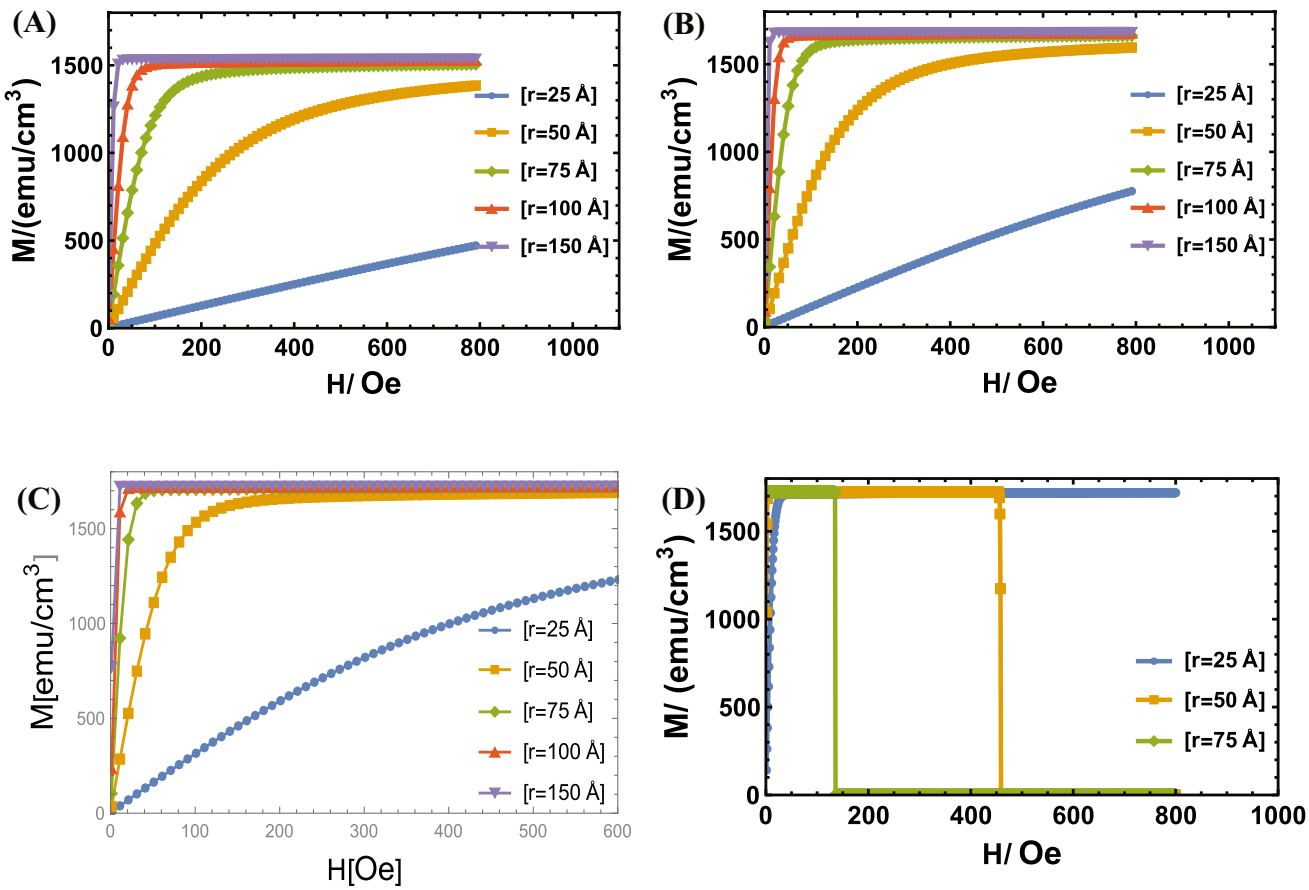

Fig. 4 The isothermal magnetization curves along [100] axis at **A** 600 K, **B** 400 K, **C** 150 K, and **D** 4 K for Fe particles of different sizes in the 25–150-Å range

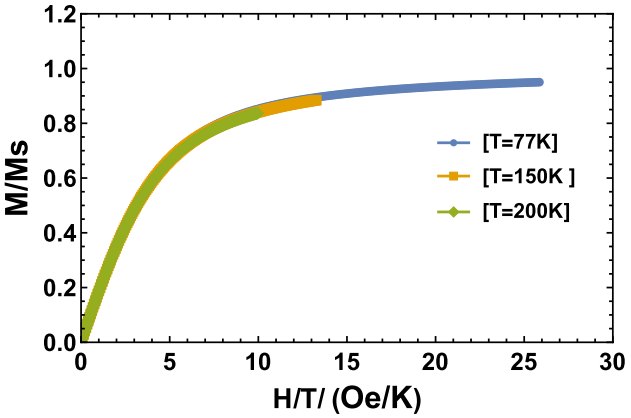

Fig. 5 Fractional magnetization as function of *H*/*T* for a 25 Å particle at $T = 77$, 150, and 200 K in a magnetic field up to 2 kOe

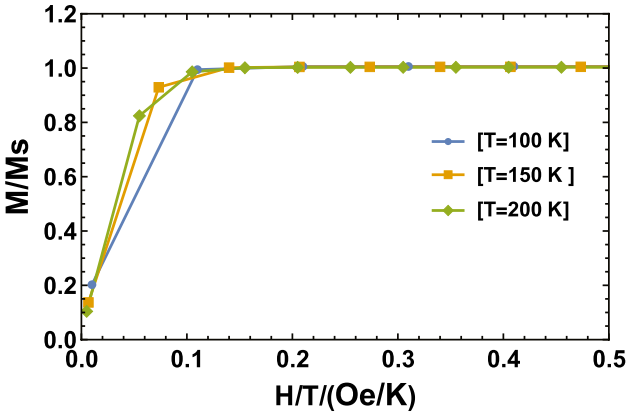

Fig. 6 Fractional magnetization as function of *H*/T for a 100 Å particle at $T = 100$, 150 and 200 K in a magnetic field up to 1 kOe

saturation increases as the particle size decreases, for these three temperatures 600, 400, and 150 K.

In addition, for particle radii in the range 25–75 Å and at 4 K, a significant increase in the saturation magnetization has been achieved, e.g., for a radius of 25 Å, the magnetization is raised to ~ 1700 emu/cm^3 as shown in Fig. 4D. This behavior is expected because thermal energy is insufficient, at low temperatures, to reduce the magnetization of extremely small particles, whereas this effect becomes more significant at high temperatures. A common feature of super-paramagnetic single-domain particles is that at high temperatures, the thermal energy overcomes the magnetic anisotropy energy barrier [29]. The most remarkable feature of superparamagnetism is shown in Fig. 5, namely the

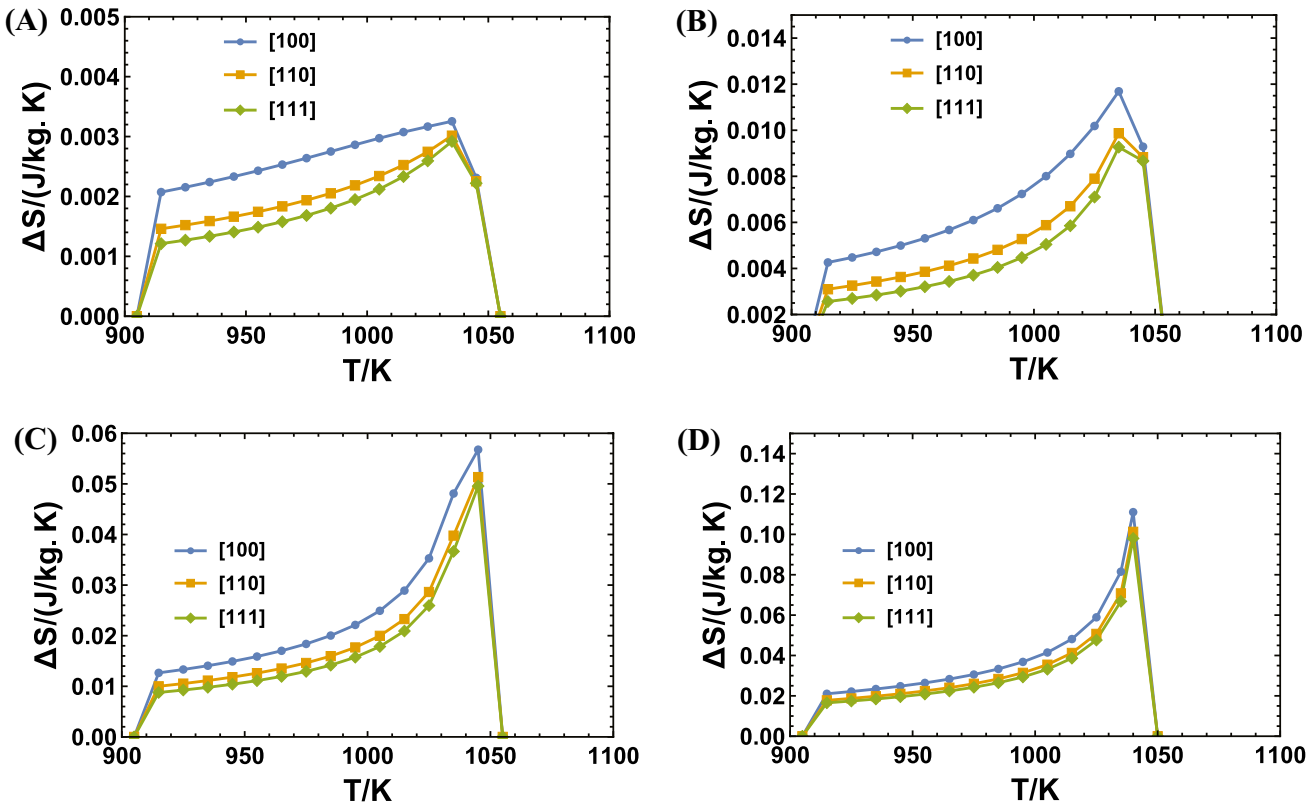

Fig. 7 The isothermal AMCE ΔS_{anis} for $r = 150$ Å, in the temperature range from 900 to 1050 K for applied fields of **A** 50 Oe, **B** 100 Oe, **C** 300 Oe, and **D** 500 Oe

Table 1 The maximum values of anisotropic ΔS_m which represents the difference between the anisotropic ΔS of the easy [100] and hard [111] directions, at different fields and for a radius of 150 Å

H (Oe)	ΔS_m *(J/K.kg) [100]*	ΔS_m *(J/K.kg) [111]*	The maximum anisotropic $\Delta S_{anisotropic}$
50	0.002	0.001	0.001
100	0.011	0.009	0.002
300	0.037	0.022	0.015
500	0.112	0.096	0.016

overlap of the M/M_s vs. H/T curves at 77, 150, and 200 K for the critical particle radius of 25 Å. The same behavior was previously pointed out in Fe, iron oxide–based alloys [58], and Gd element [29]. In contrast, Fig. 6 displays curves at temperatures 100, 150, and 200 K for size radius of 100 Å. The behavior confirms the ferromagnetic state for Fe particles [57].

3.2 Anisotropic Magnetocaloric Effect (AMCE)

The anisotropic MCE effect is manifested in the difference between the isothermal entropy changes calculated along different crystallographic directions in a field of constant magnitude [59, 60]. Figure 7A–D display the AMCE, using the trapezoidal method, in the field range 50–500 Oe, and at temperatures between 900 and 1050 K, for Fe particles of size 150 Å. The anisotropic ΔS_{anis} can be calculated by taking the difference between ΔS_m along the easy and hard directions. A large ΔS_{anis} is achieved in the low field region 50–500 Oe because the entropy of the spins is changed by application of a small field, in cluster and superparamagnetic materials more easily than in paramagnetic systems [61]. Table 1 shows the maximum value of ΔS_m at different fields 50, 100, 300, and 500 Oe for a radius of 150 Å. Figure 8

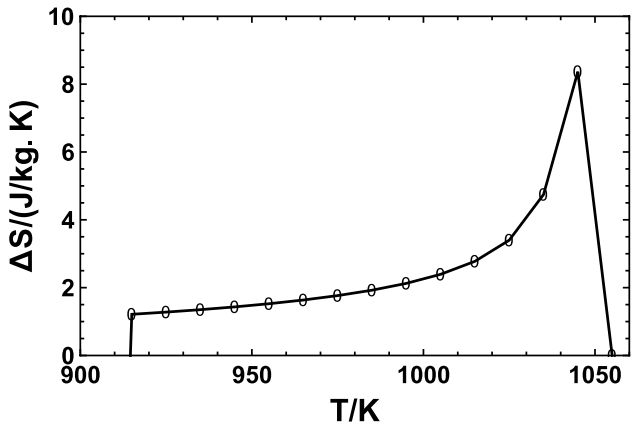

Fig. 8 The isothermal AMCE ΔS_{anis} for $r = 150$ Å, in the temperature range from 900 to 1050 K for applied fields at 30 kOe along [100]

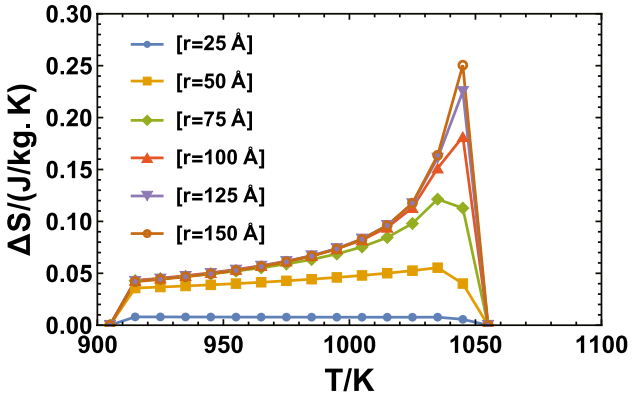

Fig. 9 ΔS_{anis} vs. temperature at $H = 1$kOe, along [100], for particles of sizes in the 25–150-Å range

displays the temperature dependence of ΔS_m for $r = 150$ Å in a field of 30 kOe. The maximum value is 8.36 J/kg K, along the easy axis, in comparison with 7.95 J/kg K for the bulk Fe [16]. So, the anisotropic MCE is enhanced over the ordinary MCE. Figures 9 and 10 display the size-dependent ΔS, in a 1kOe field along the [100] direction for radii in the range 25–150 Å. A plateau feature [51] is found for 25-Å particles almost in the whole temperature range. Table 2 shows the RCP values for radii 50, 75, 100, and 150 Å in a field of 1 kOe. The highest value of RCP is 8.11 J/kg for a radius of 50 Å.

This behavior was reported previously in nano-sized Gd element by Miller [62] and Belo et al. [21]. However, the previous studies have not taken into account the calculation of anisotropic ΔT_{ad} and only the conventional ΔT_{ad} was presented experimentally as reported by [8, 15]. Based on Eq. (9), the anisotropic ΔT_{ad} is calculated along the easy direction [100] for applied field of 30 kOe. The heat capacity data was obtained from the experimental work presented in [8]. The anisotropic ΔT_{ad} has been calculated, using our model, with maximum value of 8 K as

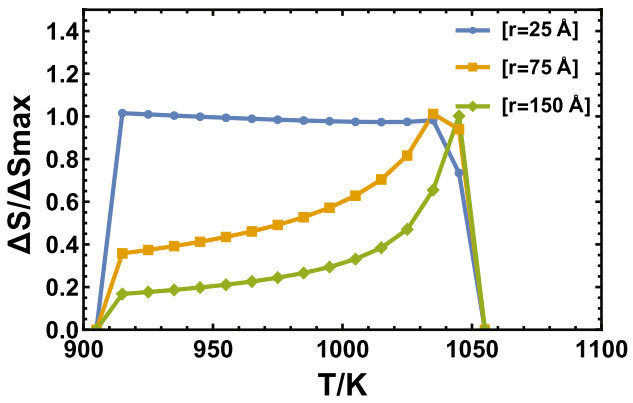

Fig. 10 The AMCE vs. temperature at $H = 1$kOe for particles of sizes of 25, 75, and 150 Å along [100] direction

Table 2 The relative cooling power RCP for Fe particles of different radii along the easy axis [100] for a field of 1 kOe

r (Å)	δT_{FWHM}	ΔS_{Max} (*J/K.kg*)	RCP (J/kg)
50	135	0.06	8.11
75	65	0.12	7.80
100	38	0.18	6.84
150	23	0.25	5.75

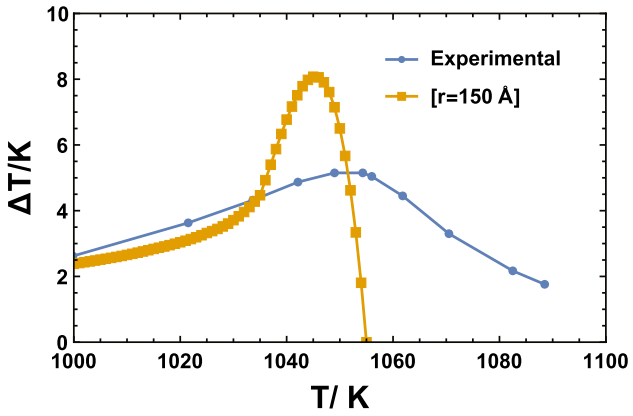

Fig. 11 The adiabatic AMCE ΔT_{anis} along [100] easy axis for $r = 150$ Å, in the temperature range from 1000 to 1050 K for applied fields of 30 kOe compared to the conventional experimental ΔT

compared to the experimental value of 5 K as shown in Fig. 11. The increase in the value of anisotropic ΔT_{ad} relative to ordinary MCE confirms the importance of applying a field along a specific crystallographic direction for obtaining a high adiabatic temperature change at the same field intensity.

4 Conclusions

The size-dependent magnetization curves for Fe particles showed a ferromagnetic behavior at room temperature, for radii in the 50–150-Å range. Particles with a smaller radius, about 25 Å, exhibit a super-paramagnetic behavior. The isothermal change in entropy for field change in the 50–500-Oe range showed an anisotropy in the ΔS_m behavior for field applied along the [100], [110], and [111] axes. The particles in the 25-Å size range exhibit a plateau in its temperature dependence of ΔS_m. The adiabatic change in temperature ΔT_{ad}, along the [100] axis, in a 30-kOe field, is about 37.5% larger than the experimental value. The lack of experimental data on $C_{\text{total}}(T, H)$ does not enable us to calculate ΔT_{ad} without the use of the approximation form of Eq. (9).

The statistical mechanics model proved to be fairly suitable for calculating the magnetothermal, magnetic size-dependent, and anisotropic magnetocaloric properties of the iron element.

Funding Open access funding provided by The Science, Technology & Innovation Funding Authority (STDF) in cooperation with The Egyptian Knowledge Bank (EKB). This project is supported financially by the Academy of Scientific Research and Technology (ASRT), Egypt, Grant No. 6701; ASRT is the 2nd affiliation of this research.

Data Availability This manuscript has no associated data or the data will not be deposited. The reader may contact me through my email: (eldocahmed4@gmail.com).

References

1. Li, L.-W.: Chinese Phys. B **25**, 37502 (2016)
2. Wei, Z., Chak-Tong, A., You-Wei, D.: Chinese Phys. B **22**, 57501 (2013)
3. Pecharsky, V.K., Gschneidner, K.A., Jr.: Int. J. Refrig. **29**, 1239 (2006)
4. Pecharsky, V.K., Gschneidner, K.A., Jr.: J. Magn. Magn. Mater. **200**, 44 (1999)
5. Franco, V., Blázquez, J.S., Ingale, B., Conde, A.: Annu. Rev. Mater. Res. **42**, 305 (2012)
6. Kuz'min, M.D., Tishin, A.M.: Cryogenics (Guildf). **32**, 545 (1992)
7. De Oliveira, N.A., von Ranke, P.J.: Phys. Rep. **489**, 89 (2010)
8. Tishin, A.M., Spichkin, Y.I.: *The magnetocaloric effect and its applications* (CRC Press, 2016)
9. Smith, A.: Eur. Phys. J. H **38**, 507 (2013)
10. Pecharsky, V.K., Gschneidner, K.A., Jr., Pecharsky, A.O., Tishin, A.M.: Phys. Rev. B **64**, 144406 (2001)
11. Lyubina, J.: J. Phys. D. Appl. Phys. **50**, 53002 (2017)
12. Gschneidner, K.A., Jr., Pecharsky, V.K.: Annu. Rev. Mater. Sci. **30**, 387 (2000)
13. Smith, A.: Energy Mater **2**, 1288 (2012)
14. Ram, N.R., Prakash, M.: J. Supercond. Nov. Magn **31**, 1971 (2018)
15. Tishin, A.: Cryogenics **30**, 127 (1990)
16. De Oliveira, N.A.: J. Alloys Compd. **403**, 45 (2005)
17. Kuz'min, M.D., Tishin, A.M.: J. Appl. Phys. **73**, 4083 (1993)
18. Hamad, M.A.: J. Supercond. Nov. Magn. **29**, 1539 (2016)
19. Zarkevich, N.A., Zverev, V.I.: Crystals **10**, 815 (2020)
20. da Cal Seixas, S.R., de Moraes Hoefel, J.L.: (n.d.)

21. Belo, J.H., Pires, A.L., Araújo, J.P., Pereira, A.M.: J. Mater. Res. **34**, 134 (2019)
22. Balli, M., Mansouri, S., Jandl, S., Fournier, P., Dimitrov, D.Z.: Magnetochemistry **3**, 36 (2017)
23. Orendáč, Matúš, et al.: Rotating magnetocaloric effect and unusual magnetic features in metallic strongly anisotropic geometrically frustrated TmB4. Sci. Rep. **8.1**, 1–10 (2018)
24. Huang, J., Li, Y., Orza, A., Lu, Q., Guo, P., Wang, L., Yang, L., Mao, H.: Adv. Funct. Mater. **26**, 3818 (2016)
25. Li, R.-N., Da, X.-H., Li, X., Lu, Y.-S., Gu, F.-F., Liu, Y.: Chinese Phys. B **30**, 17502 (2021)
26. Tishin, A.M., Spichkin, Y.I.: Int. J. Refrig. **37**, 223 (2014)
27. Tishin, A.M., Spichkin, Y.I., Zverev, V.I., Egolf, P.W.: Int. J. Refrig. **68**, 177 (2016)
28. Kumar, C.S.S.R., Mohammad, F.: Adv. Drug Deliv. Rev. **63**, 789 (2011)
29. Aly, S.H.: J. Magn. Magn. Mater. **222**, 368 (2000)
30. Aly, S.H., Yehia, S., Soliman, M., El-Wazzan, N.: J. Magn. Magn. Mater. **320**, 276 (2008)
31. Aly, S.H., Yehia, S.: J. Magn. Magn. Mater. **202**, 565 (1999)
32. Sobh, H.A., Aly, S.H.: Chinese Phys. B **26**, 17503 (2017)
33. Yehia, S.: J.MMM **212**, 195 (2000)
34. Bozorth, R.M.: J. Appl. Phys. **8**, 575 (1937)
35. O'handley, R.C.: Modern magnetic materials: principles and applications (Wiley, 2000)
36. Wohlfarth, E.P.: Handbook. Ferromagn. Mater. **1**, 1 (1980)
37. Kittel, C., McEuen, P.: Kittel's introduction to solid state physics (John Wiley & Sons, 2018)
38. Cullity, B.D., Graham, C.D.: Introduction to magnetic materials (John Wiley & Sons, 2011)
39. Klein, H.-P., Kneller, E.: Phys. Rev. **144**, 372 (1966)
40. Getzlaff, M.: Fundamentals of magnetism (Springer Science & Business Media, 2007)
41. Callen, H.B., Callen, E.: J. Phys. Chem. Solids **27**, 1271 (1966)
42. Callen, E.R.: J. Appl. Phys. **33**, 832 (1962)
43. Piety, R.G.: Phys. Rev. **50**, 1173 (1936)
44. Skomski, R., Mryasov, O.N., Zhou, J., Sellmyer, D.J.: J. Appl. Phys. **99**, 08E916 (2006)
45. Khedr, D.M., Aly, S.H., Shabara, R.M., Yehia, S.: J. Magn. Magn. Mater. **430**, 103 (2017)
46. Hesham, R., Aziz, M.A., Yehia, S., Ghani, A.A.: Cryogenics **115**, 103229 (2021)
47. Elkenany, M.M., Aly, S.H., Yehia, S.: Cryogenics (Guildf). **123**, 103439 (2022)
48. Lee, J.S.: Phys. Status Solidi **241**, 1765 (2004)
49. Pecharsky, V.K., Gschneidner, K.A., Jr.: J. Appl. Phys. **86**, 565 (1999)
50. Földeàki, M., Chahine, R., Bose, T.K.: J. Appl. Phys. **77**, 3528 (1995)
51. Cahn, R.: Intermetallic compound: principle and practices, volume3, progress (2002)
52. Coey, J.M.D.: Magnetism and magnetic materials (Cambridge university press, 2010)
53. Kittel, C., McEuen, P., McEuen, P.: Introduction to solid state physics. Wiley, New York (1996)
54. Crangle, J., Goodman, G.M.: Proc. R. Soc. London. A. Math. Phys. Sci. **321**, 477 (1971)
55. Suryanarayana, C.: Int. Mater. Rev. **40**, 41 (1995)
56. Birringer, R.: in *Proc*. Japan Inst. Met. Int. Symp. **2**, 43–52 (1986)
57. Bean, C.P., Livingston, J.D.: J. Appl. Phys. **30**, S120 (1959)
58. Yamamoto, T.A., Tanaka, M., Misaka, Y., Nakagawa, T., Nakayama, T., Niihara, K., Numazawa, T.: Scr. Mater. **46**, 89 (2002)
59. von Ranke, P.J., De Oliveira, N.A., Garcia, D.C., De Sousa, V.S.R., De Souza, V.A., Carvalho, A.M.G., Gama, S., Reis, M.S.: Phys. Rev. B **75**, 184420 (2007)
60. Plaza, E.J.R., De Sousa, V.S.R. et al.: J. Appl. Phys. **105**, 13903 (2009)
61. McMichael, R.D., Shull, R.D., Swartzendruber, L.J., Bennett, L.H., Watson, R.E.: J. Magn. Magn. Mater. **111**, 29 (1992)
62. Miller, C.W., Belyea, D.D., Kirby, B.J.: J. Vac. Sci. Technol. **32**, 40 (2014)